Research Article

Journal of Environmental Nanotechnology

Investigation on Pure and Aluminium-doped Hydroxyapatite for Orthopedic Applications

V. Kalaiselvi*, T. Loganayaki, M. Nathiya
Department of Physics, Navarasam Arts & Science College for Women, Arachalur, Erode, TN, India
Received: 28.01.2021 Accepted: 03.03.2021 Published: 30-01-2021
*nk.arthikalai@gmail.com

ABSTRACT

In the present work, synthesis and characterization of pure and Aluminium-doped Hydroxyapatite nanoparticles were performed. Biomaterials were selected owing to their bone replacement applications. The main proposition of this work is to synthesize the Hydroxyapatite (HAp) nanoparticles by microwave-assisted co-precipitation method at room temperature. The prepared samples were characterized by using various techniques such as Powder XRD, SEM, EDAX, UV-Visible, Photoluminescence (PL) and FT-IR methods. The antimicrobial analysis was performed to study the crystalline size, micro-strain and dislocation density of the samples. SEM revealed the morphology of the samples. The composition of the samples was revealed by EDAX, whereas UV and PL have thrown light upon the optical property of the samples. Functional groups were determined by FTIR. Zone of inhibition for gram-positive and gram-negative bacteria was shown by antimicrobial analysis.

Keywords: EDAX; FT-IR; Hydroxyapatite; Nanomaterials; SEM; UV-Visible; XRD.

1. INTRODUCTION

This Calcium phosphates come under the community of ceramic material, which is widely used to treat orthopaedic defects. Especially, Hydroxyapatite based ceramic material is considered as one of the potential calcium–phosphate candidates for bone and bone-related clinical applications because of its chemical composition being closely related to that of the mineral phase of bone (Amogh Tathe *et al.* 2014; Vignesh Raj *et al.* 2018).

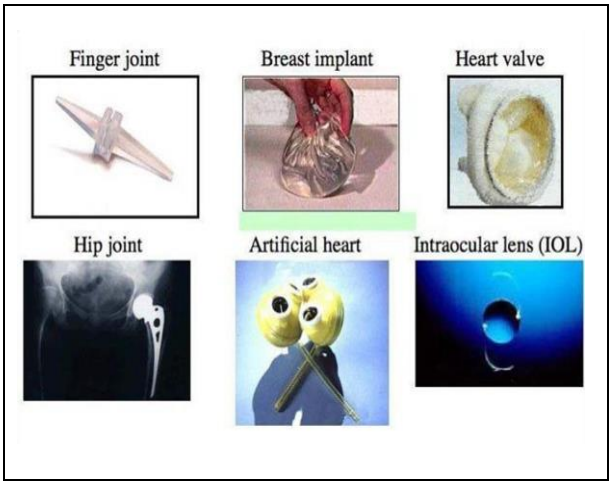

Fig. 1: Common medical devices comprised of biomaterials

However, many physical and mechanical properties of hydroxyapatite, including bioactivity, biocompatibility, solubility, sinterability, castability, fracture toughness and absorption can be tailored over wide ranges by controlling the particle composition, size and morphology. Hence it is of great importance to developing synthesis methods focused on the precise control of particle size, morphology and chemical composition of Hydroxyapatite. The metal-doped Hydroxyapatite particles at the nanoscale level have a greater impact owing to their smaller size and larger specific surface area, enabling homogeneous resorption by osteoclasts (Gopi *et al.* 2012; Rajendran *et al.* 2014).

Focus has been laid this work on the synthesis and characterization of pure and Al-doped HAp nanoparticles in view of their bone replacement applications. The main proposition of this work is to synthesize the HAp nanoparticles by microwave-assisted co-precipitation method at room temperature. The prepared samples were characterized by using various techniques such as Powder XRD, SEM, EDAX, UV-Visible, PL, FT-IR and Antimicrobial methods. The antimicrobial analysis was performed to study the *in-vitro* analysis of the samples (Kanimozhi *et al.* 2014; Kalaiselvi *et al.* 2017).

2. MATERIALS AND METHODS

2.1 Synthesis of HAp Nanoparticles

HAp nanoparticles were prepared by the microwave irradiation method. 1 M of calcium hydroxide, 0.6 M of orthophosphoric acid, 0.3 M of Triethonalamine were dissolved in 100 ml of distilled water and stirred at room temperature for 1 hour. The

H_3PO_4 was added with drop by drop in $Ca(OH)_2$ solution at room temperature. The capping agent is added to the mixture of $Ca(OH)_2$ and H_3PO_4 solution. Ammonia solution was added dropwise to the mixture with constant stirring. This mixture was continuously stirred for 6 hours. These final products were allowed to cool for 24 hours with the help of an ice cube. This aged precipitate is washed with distilled water. Finally, the white product was kept in a microwave oven at 70 $^{\circ}$C for 15 to 20 minutes. The dried sample was grained in a mortar and pestle to get white-color HAp nanopowder.

2.2 Synthesis of Aluminium-doped HAp Nanoparticles

Aluminium-doped HAp nanoparticles were prepared by the microwave irradiation method. 0.9 mol of $Ca(OH)_2$, 0.6 mol of H_3PO_4, capping agent 0.3 mol of TEA, 0.1 mol of aluminum was dissolved in 100 ml of distilled water under stirring at room temperature for 1 hour separately. The H_3PO_4 and aluminum solution was added drop by drop in calcium hydroxide solution at room temperature. And then, the capping agent is added to the mixture of $Ca(OH)_2$, H_3PO_4 and aluminum solution. Ammonia solution was added dropwise to the mixture, under stirring. This mixture was continuously stirred for 6 hours at room temperature. These final products were allowed to cool for 24 hours using an ice cube. This aged precipitate is washed with distilled water. Finally, the white product was kept in a microwave oven at 70 $^{\circ}$C for 15 to 20 minutes. The dried sample was grained in a mortar and pestle to get white-color Al-doped HAp nanopowder.

3. RESULTS AND DISCUSSION

3.1 XRD

The XRD analysis of the prepared sample of pure Hap and Al-doped Hap nanoparticles was done by powder X–Ray diffraction using CuKα as X-Ray Source (λ=1.5406 A^o). Fig. 2 represents the X-ray diffraction pattern of pure and Al-doped HAp nanoparticles. From fig. It is evident from the figure that some major peaks emerge, which indicates the crystalline nature. HAp possesses a polycrystalline structure. The strong diffraction peaks in the XRD spectrum of pure and Al-doped HAp nanoparticles occurring at 2θ values 10.5^o, 25.8^o, 32.1^o, 32.8^o, 34^o and 49.6^o are indexed as the (100), (002), (112), (300), (202), (213) crystal planes and correspond to the hexagonal structure of HAp with lattice constant a=9.42A^o and c=6.879A^o, which is consistent with the standard [JCPDS (74-566)] data (Table 1). No other impurity peaks were detected. The absence of any peak from aluminum confirms that Al acts as a substitutional dopant. A slight broadening and decrease in the maximum intensity of the peaks were noticed by adding Al dopant in the HAp lattice. The average grain size of the nanoparticles can be calculated using Debye-Scherrer's formula,

$$D=K\lambda/ \beta \cos \theta$$

where,

'D' is the mean crystallite size,
'K' is the shape factor taken as 0.9,
'λ' is the wavelength of monochromatic X-Ray beam(nm),
'β' is the FWHM (full width at half maximum) for the diffraction peak under consideration (in radians) and 'θ' is the diffraction angle (^{o}).

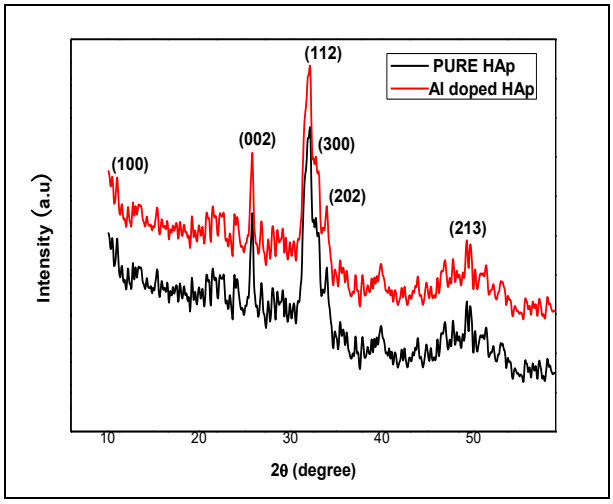

Fig. 2: XRD patterns of pure and Al-doped HAp nanoparticles

Table 1. The crystalline size for pure HAp nanoparticles

Sample	2θ (deg.)	Crystalline size D (nm)	Average crystalline size (nm)
Pure HAp	10.5228	59.0814	35-67
	25.8210	24.7808	
	32.1206	63.3882	
	32.7789	66.9446	
	33.9691	38.9917	
	49.6207	35.1805	
Al-doped HAp	10.5233	55.9851	35-77
	25.8213	24.2424	
	32.1213	73.0521	
	32.7684	77.4670	
	33.9713	37.9573	
	49.6739	35.1557	

The formula determines the microstrain of the HAp nanoparticles,

$$E_{strin} = \beta/ 4 \tan \theta$$

where,

'β' is the full width at half maximum for the diffraction peak (002) (in radians) and

'θ' is the diffraction angle (°) for the peak (002) (Table 2).

The formula determines the Dislocation density of the HAp nanoparticles,

$$\delta = 1/D^2$$

where,

'D' is the crystalline size in nm

Table 2. Microstrain and Dislocation Density for Pure and Al-doped HAp

Sample	2θ	hkl	E_{strin} x 10^{-3}	Dislocation density, δ x 10^{15}
Pure HAp	25.8°	(002)	6.25817	1.628
Al-doped HAp	25.8°	(002)	6.40856	1.701

The micro-strain, as well as the dislocation density, is increased with the addition of dopant Al into the pure HAp nanoparticles.

3.2 SEM Analysis

The Morphology and crystallite size of the particles were investigated by SEM. The SEM image of the HAp nanoparticles in Fig. 3(a) clearly shows that the as-prepared HAp nanoparticles have a spherical shape and uniform size. Their average size varied from 52-66 nm.

SEM image of Al-doped HAp nanoparticles shows their non-homogeneity; non-uniform agglomerates of elongated, spherical shapes and plate type shapes were found (Fig. 3b). The particles size varies from 61-90 nm.

3.3 EDAX (Energy-Dispersive X-Ray Spectroscopy)

The elemental composition of pure HAp and Al-doped HAp nanoparticles was carried out by EDAX spectroscopy. Fig. 4 (a) and Fig. 4 (b) reveal the EDAX spectrum of pure and Al-doped HAp nanoparticles. The strong peaks observed in the spectrum of Fig. 4 (a). are due to Ca, P and O. The prepared HAp nanoparticles to have an atomic percentage of 72.25 of Oxygen, 9.84 of Phosphorus and 17.90 of Calcium, confirming the formation of HAp nanoparticles. The strong peaks observed in the spectrum of Fig. 4(b) are due to Ca, P, O and Al for doped HAp. The prepared Al-doped HAp nanoparticles have an atomic percentage of 75.99 of Oxygen, 9.28 of Phosphorus, 13.69 of Calcium and 1.04 of aluminum (Table 3), which confirms the presence of a small amount of aluminum in the HAp lattice.

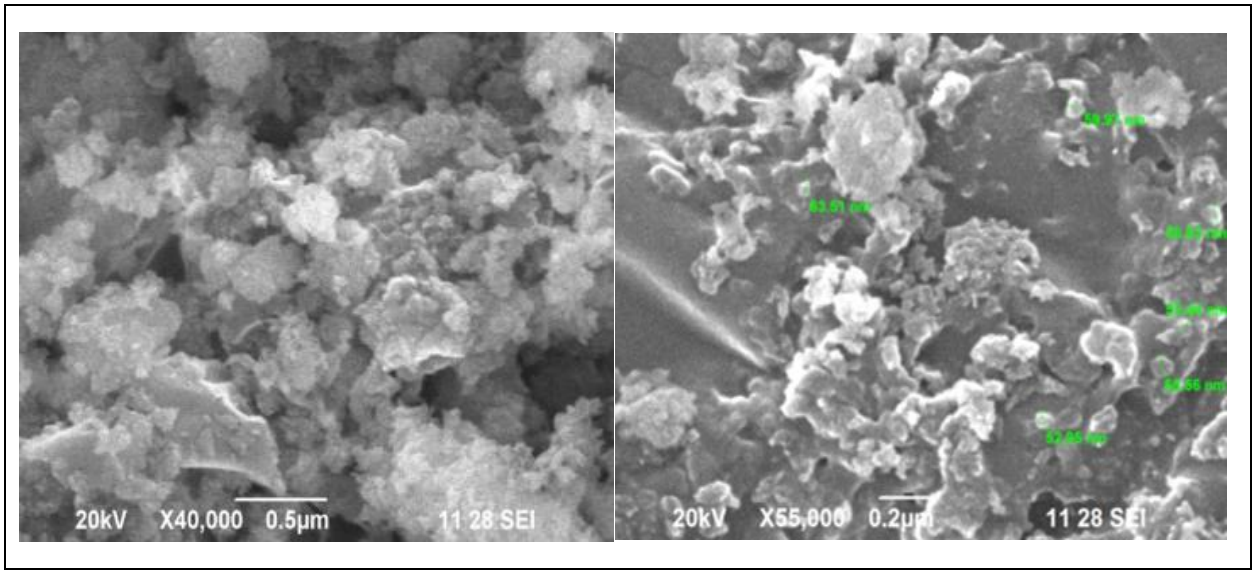

Fig. 3 (a): SEM images of pure HAp nanoparticles

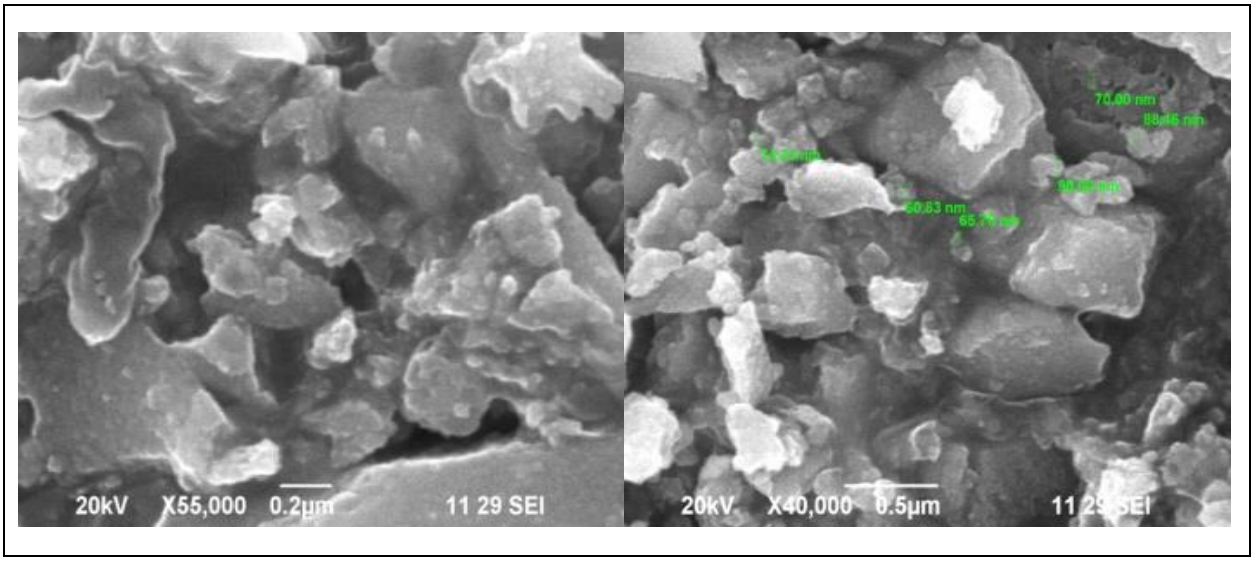

Fig. 3 (b): SEM images of Al-doped HAp nanoparticle

Table 3. The atomic content of pure and doped Nanoparticles from EDAX measurements

Type of nanoparticles	EDAX results			
	Ca (%)	P (%)	O (%)	Aluminum (%)
Pure HAp	17.90	9.84	72.25	-
Al-doped HAp	13.69	9.28	75.99	1.04

3.4 FTIR Analysis

The FTIR spectrum of Pure and Al-doped HAp nanoparticles were recorded by using Perkin-Elmer Spectrometer in the range of 400-4000 cm^{-1}, using KBr pellet technique, in order to identify the functional groups. The broad peaks at 3432 cm^{-1} and 1642 cm^{-1} in the spectrums (Pure and Al-doped) can be attributed to the absorbed water, while the sharp peak at 3368 cm^{-1} was attributable to the stretching vibrations of the lattice OH^- ions and the medium sharp peak at 633 cm^{-1} can be ascribed to the OH- deformation mode. The peak at 1636 cm^{-1} can be attributed to the bending mode of water. The intense broad peak between 900 cm^{-1} and 1100 cm^{-1} was because of the stretching mode of PO_4^{3-}. The bending modes of PO_4^{3-} appeared at 602 cm^{-1} and 562 cm^{-1} as intense sharp peaks. The bands with a shoulder at 962 cm^{-1} - 1105 cm^{-1} were due to the P-O stretching vibrations of the Phosphate groups. The weak band at about 470 cm^{-1} corresponds to the Phosphate bending vibration. The peak at 873 cm^{-1} was caused by HPO_4^{2-} groups. The CO_3^- derived bands were observed at 1402 cm^{-1} - 1460 cm^{-1}. It might be due to the absorption of an atmospheric Carbon-di-oxide during the sample preparation. The medium sharp peak at 902 cm^{-1} was assigned to Al-O stretching mode (Table 4).

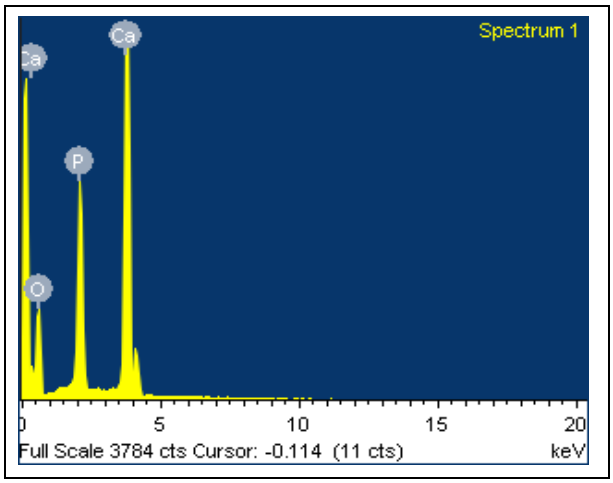

Fig. 4(a): Pure HAp

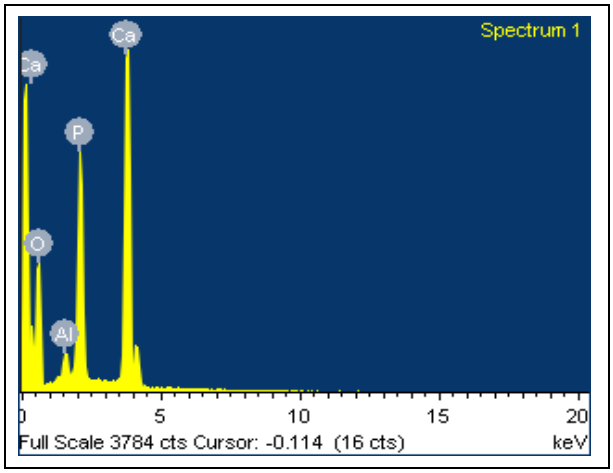

Fig. 4(b): Al-doped HAp

Table 4. Chemical functional groups using FTIR

Assignments	Functional groups cm^{-1}	
	Pure HAp (cm^{-1})	Al-doped HAp (cm^{-1})
OH –Stretching mode	3368	3415
H_2O – Bending mode	1646	1645
PO_4^{3-} - Stretching mode	1033	1041
PO_4^{3-} - Bending mode	565 & 602	565 & 603
PO - Stretching mode	962	963.85
PO - Bending mode	471	472
HPO_4^{2-}	873	875
Al-O - Stretching mode	-	901 cm^{-1}

The weak peak at 3570 cm^{-1} corresponds to the vibrations of OH^- ions in the HAp lattice. The table shows the functional groups of pure HAp and Al-doped HAp nanoparticles.

3.5 Optical Studies

3.5.1 UV-Visible Studies

The optical behavior of the nanoparticles was assessed by using UV-Visible spectrometer instruments in the range of 200-1100 nm. An optical absorbance spectrum is shown in Fig. 5 (a) and 5 (b). The figure shows the UV-Visible spectra of pure and Al-doped HAp nanoparticles. The lower cut-off wavelength at 237.4 nm for pure HAp nanoparticles and 234.7 nm for Al-doped HAp nanoparticles indicate the absorbance in the entire UV-Visible region of the spectrum. The bandgap energies were calculated using the formula:

$$E_v = h\gamma$$
$$E_v = hc/\lambda$$

where,

'h' is Plank's constant
'c' is the velocity of light and
'λ' is the wavelength in nm

The bandgap energy for the spectra of pure HAp nanoparticles is 5.2 eV. When the dopant Al was added to pure HAp nanoparticles, the bandgap energy is slightly increased from 5.2 eV to 5.3 eV. This variation of bandgap energy was not affecting the conductivity. The absorption of the compound is due to the n-π^* transitions. Hence the compound may be useful for the fabrication of optical materials.

3.5.2 Photoluminescence Studies

The Photoluminescence spectrum occurred when the electron absorbed energy and was raised to an excited state. The excited state electrons were returned to the ground state by the emission of radiation. The Photoluminescence spectra for pure HAp nanoparticles and Al-doped HAp nanoparticles, shown in Fig. 6 (a) and (b), were recorded using a Perkin-Elmer LS45 model spectrometer in the range from 280 nm to 900.5 nm. The observed sharp emission peaks at 529 nm represent pure HAp nanoparticles and 530 nm for Al-doped HAp nanoparticles. The pure HAp and Al-doped HAp nanoparticles spectrum indicate the emission of green light.

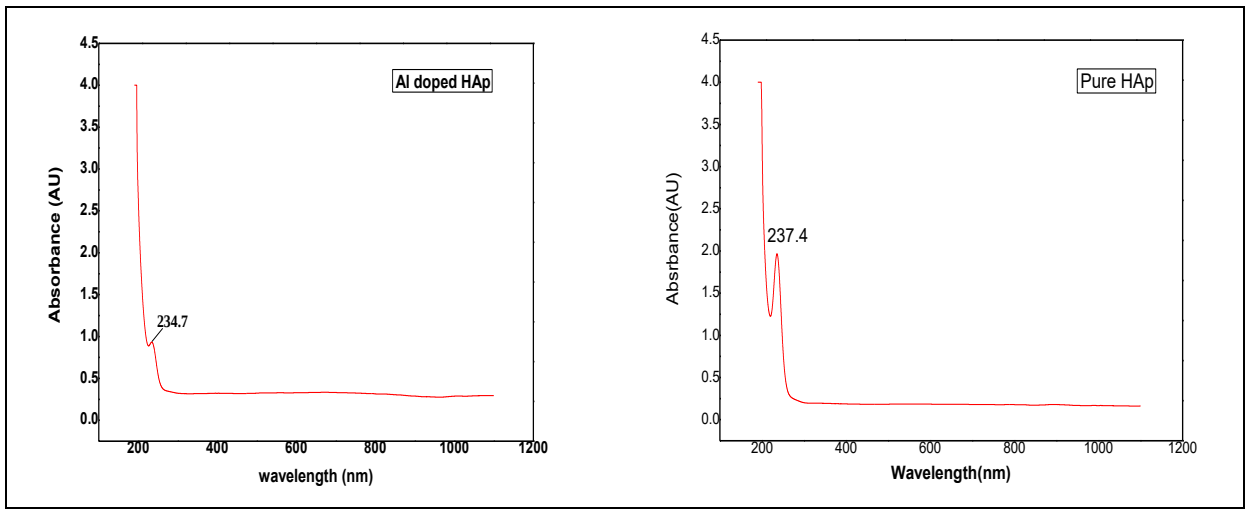

Fig. 5 (a) & (b): UV spectrum of pure and Al-doped HAp nanoparticles

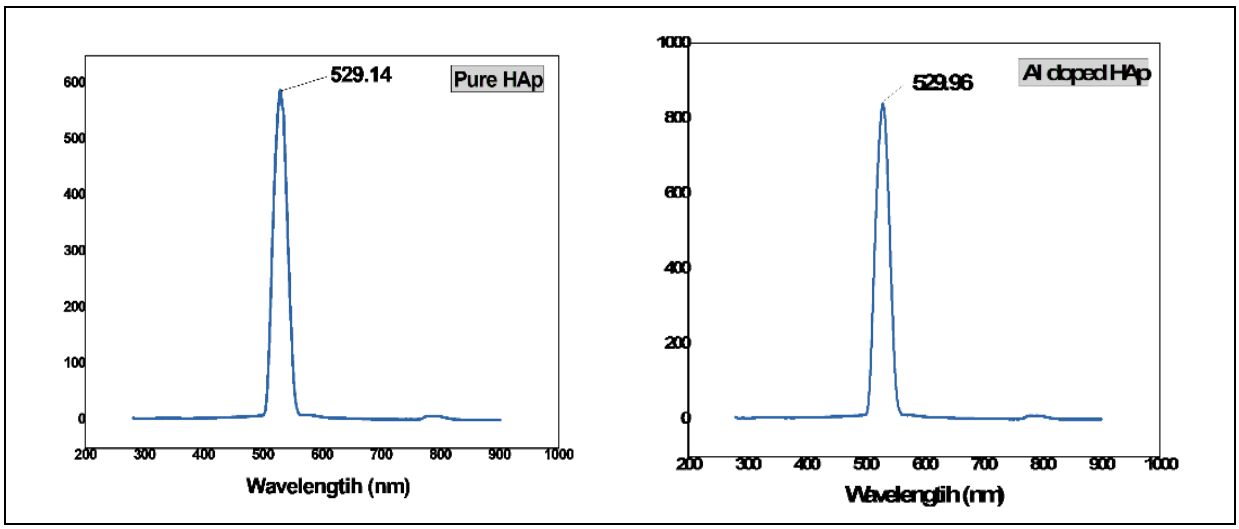

Fig. 6 (a) & (b): Photoluminescence spectra of pure and Al-doped HAp nanoparticles

3.6 Antibacterial Studies

The agar well diffusion method was employed in antibacterial studies for prepared nanoparticles (Sriram *et al*. 2014). The antibacterial activity of the nanoparticles was tested against the gram-positive strains - *Staphylococcus aureus*, gram-negative *Escherichia coli* and gram-negative *Staphylococcus epidermidis*. The zone of inhibition diameter values of the nanoparticles was determined and shown in Table 5.

Table 5. Zone of inhibition diameter of HAp nanoparticles (mm)

Strains	Zone of Inhibition diameter (mm)					
	Pure HAp		Al-doped HAp			
Concentrations	75	100	25	50	75	100
Staphylococcus aureus	0	0	0	0	0	0
Escherichia coli	4	5	0	0	3	5
Staphylococcus epidermidis	0	0	3	4	5	6

The zone of Inhibition diameter values was measured for four different concentrations (25, 50, 75 and 100 µg/ml). The bacterial inhibition was increased with an increase in the concentration of nanoparticles (Fig.7). *Staphylococcus aureus* and *Staphylococcus epidermidis* were gram-positive bacteria. *Escherichia coli* is a gram-negative bacterium. The pure HAp nanoparticles were effective on the gram-negative bacterium. The aluminum-doped HAp nanoparticles were efficient on gram-positive bacterium of *Staphylococcus epidermidis*. The antibacterial effect of pure HAp nanoparticles was superior on *Escherichia coli* than other strains.

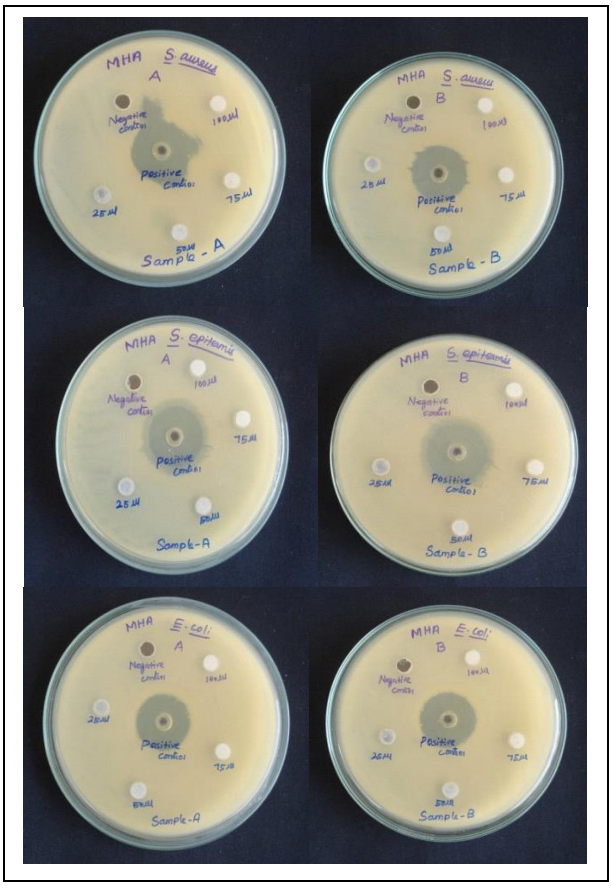

Fig. 7: Inhibition plates of sample A – Pure HAp and sample B–Al-doped HAp

The antibacterial effect of aluminum-doped HAp nanoparticles was superior on *Staphylococcus epidermidis* than on other strains. But gram-positive bacterium of *Staphylococcus aureus* has no activity on

pure HAp and Al-doped HAp nanoparticles. In furthermore concentrations, it may have an impact on the bacteria. Thus, HAp can be used for orthopedic applications.

4. CONCLUSION

Hydroxyapatite is the main biomaterial used in the field of orthopedic applications. Hydroxyapatite and Aluminium-doped Hydroxyapatite nanoparticles were synthesized by the microwave-assisted co-precipitation method. Biomaterials with aluminum dopant were applied for the present study in view of their bone replacement applications. The main proposition of this work is to synthesize the pure Hydroxyapatite and Aluminium-doped Hydroxyapatite nanoparticles at room temperature. The prepared samples are characterized using various techniques such as Powder XRD, SEM, EDAX, UV-Visible, PL and FT-IR methods. The antimicrobial analysis was performed to study the *in-vitro* analysis of the samples. XRD reveals the crystalline size, micro-strain and dislocation density of the samples in the expected range. SEM revealed the spherical-shaped morphology in both samples. The presence of Ca, P, O and Al under a proper proportion of 1.6 was revealed by EDAX. UV and PL revealed the bandgap and excitation wavelength of the samples. Functional groups were determined by FTIR. Zone of inhibition for gram-positive and gram-negative bacteria was shown by antimicrobial analysis. Gram-negative bacteria have significant ZOI for all the samples. Thus we conclude Hydroxyapatite and Al-doped Hydroxyapatite can be considered as highly promising candidates for orthopedic applications.

FUNDING

This research received no specific grant from any funding agency in the public, commercial, or not-for-profit sectors.

CONFLICTS OF INTEREST

The authors declare that there is no conflict of interest.

REFERENCES

Amogh Tathe, C., Ghodke, M., Nikalje, A. P. and Chavan, Y. B., A Brief review: Biomaterials and their application, *Int. J. Pharm. Pharm. Sci.*, 2(4), 19–23 (2014).

Gopi, D., Indira, J., Kavitha, L., Sekar, M. and Mudali, U. K., Synthesis of hydroxyapatite nanoparticles by a novel ultrasonic assisted with mixed hollow sphere template method, *Spectrochim. Acta Part A Mol. Biomol. Spectrosc.*, 93, 131–134 (2012). https://dx.doi.org/10.1016/j.saa.2012.02.033

Kanimozhi, K., Gopi, De'. and Kavitha, L., Synthesis and characterization of banana peel derived biopolymer/hydroxyapatite nanocomposite for biomedical applications, *Int. J. Sci. Eng. Res.*, 5(3), 138–140 (2014).

Kalaiselvi, V., Mathammal, R. and Anitha, P., Synthesis and characterization of hydroxyapatite nanoparticles using wet chemical method, *Int. J. Adv. Sci. Eng.*, 4(2), 571 (2017). https://dx.doi.org/10.29294/IJASE.4.2.2017.571-574

Rajendran, A., Barik, R. C., Natarajan, D., Kiran, M. S. and Pattanayak, D. K., Synthesis, phase stability of hydroxyapatite–silver composite with antimicrobial activity and cytocompatability, *Ceram. Int.*, 40(7), 10831–10838 (2014). https://dx.doi.org/10.1016/j.ceramint.2014.03.075

Sriram, T. and Pandidurai, V., Synthesis of silver nanoparticles from leaf extract of *Psidium guajava* and its antibacterial activity against pathogens, *Int. J. Curr. Microbiol. App. Sci.*, 3(3), 146–152 (2014).

Vignesh Raj, S., Rajkumar, M., Meenakshi Sundaram, N. and Kandaswamy, A., Synthesis and characterization of hydroxyapatite/alumina ceramic nanocomposites for biomedical applications, *Bull. Mater. Sci.*, 41(4), 93 (2018). https://dx.doi.org/10.1007/s12034-018-1612-4